Catalysis Today 181 (2012) 156–162

Contents lists available at ScienceDirect

Catalysis Today

journal homepage: www.elsevier.com/locate/cattod

Silver and gold modified plasmonic TiO_2 hybrid films for photocatalytic decomposition of ethanol under visible light

Á. Veres[a], T. Rica[a], L. Janovák[b], M. Dömök[a], N. Buzás[b], V. Zöllmer[c], T. Seemann[c], A. Richardt[d], I. Dékány[a,b,c,*]

[a] Department of Physical Chemistry and Materials Science, University of Szeged, Aradi vertanuk tere 1., H-6720 Szeged, Hungary
[b] Nanocolltech Ltd., Gogol u. 9/b, H-6722 Szeged, Hungary
[c] Fraunhofer-Institute for Manufacturing and Advanced Materials – IFAM Wiener Strasse 12, D-28359 Bremen, Germany
[d] German Armed Forces Scientific Institute for Protection Technologies – NBC-Protection, P.O. Box 1142, D-29623 Munster, Germany

ARTICLE INFO

Article history:
Received 16 March 2011
Received in revised form 21 May 2011
Accepted 30 May 2011
Available online 20 July 2011

Keywords:
Titanium dioxide
Silver
Gold
Plasmonic properties
Nanohybrid films
Photooxidation

ABSTRACT

Plasmonic noble metal nanoparticles (NPs) (silver and gold) are able to sensitise photocatalysts in visible light by modifying the TiO_2 surface with 0.5 wt% loading. These plasmonic catalysts were supported by optically transparent zirconium dioxide and layer silicate. The hybrid catalyst films (with ~10 μm thickness) were prepared by sputtering the aquatic suspension of the catalyst/support suspension on glass slides and irradiated the films by visible light ($\lambda \geq 435$ nm). The photocatalytic efficiency was studied on decomposition of ethanol vapour, and the residual concentration of ethanol was monitored. The intermediates during illumination were analysed by GC–MS. Modifications with silver and gold lead to a change in the optical properties due to the plasmonic light absorption on TiO_2. The supporting binding materials are almost transparent in UV–vis wavelength range, thus Ag- and Au-modified TiO_2 can be excited by the incoming light without much loss of the photon energy. Furthermore, the layered silicate promoted the photocatalytic process by its high adsorption capacity. Due to these two phenomena, a synergistic effect was found on the photocatalytic activity of the nanocomposite hybrid films.

1. Introduction

TiO_2 has received great attention for decades since it can be applied in many industrial processes due to its advantageous chemical and physical properties. It is also successfully used as a photocatalyst for different photooxidative applications in gas or aqueous phase. Despite its chemical inertness, non-toxic nature and low price it has a big disadvantage as it has a relatively large band gap energy (anatase, $E_g = 3.2$ eV; rutile, 3.0 eV), therefore it can only be excited by c.a. 5% of the total energy from the solar spectrum. High electron–hole recombination rate is also a disadvantage. It has been established that charge carrier recombination occurs within nanoseconds [1]. Some efforts have been made to decrease the recombination rate of electron–hole pairs by contacting other semiconductors with the catalyst. Do et al. observed enhanced photocatalytic effect in case of WO_3/TiO_2 system, which could be related to an increase in electron transfer from the TiO_2 to the outer system [2].

Visible light induced catalysts, which are also known as second generation catalysts, are sensitised to the visible region of the spectrum. It is possible to extend the absorption spectrum of TiO_2 by, for example, modifying the catalyst with different non-metallic and metallic elements. These modified catalysts can be excited by the near-UV region of the spectrum due to the absorption of metal NPs at lower energy wavelengths.

Among non-metals carbon [3], nitrogen [4], phosphorous [5–7], and fluorine [8] are used most commonly to modify photocatalysts. A wide range of metals has been successfully applied for doping TiO_2 catalyst such as iron [9,10], chromium [11], nickel [12] and noble metals [13–17]. It has been pointed out in several publications that incorporation of metal NPs enhanced photocatalytic activity [18–21]. This can be explained by two reasons. First is the shift in absorption maximum that results in reduced band gap energy. Second, the doping metal particles behave as electron traps thus they can decrease the recombination rate [22,23]. Sá et al. [24] proved that the addition of metal clusters creates a sink for photogenerated electrons, thus decreasing the rate of charge recombination. The phenomenon, called "plasmonic photocatalysis" has a wide range of interest nowadays [25]. Photocatalytic activity is greatly influenced by the amount and by the size of metal nanoparticles (NPs) used as dopants [26,27]. Accordingly, synthe-

* Corresponding author at: University of Szeged, Aradi vertanuk tere 1., H-6720 Szeged, Hungary. Tel.: +36 62 544210; fax: +36 62 544042.
E-mail address: i.dekany@chem.u-szeged.hu (I. Dékány).

0920-5861/$ – see front matter © 2011 Elsevier B.V. All rights reserved.
doi:10.1016/j.cattod.2011.05.028

sis parameters of metal NPs are crucial. Another way of increasing photocatalytic degradation is to support the catalyst over solids possessing high specific surface area, such as zeolites [28], activated carbon [29] or layered silicates [30,31].

In our previous work, we synthesised Ag-modified TiO_2 catalysts in different mass ratios of silver and characterised them by TEM, XRD, XPS and DR-UV–vis spectroscopy [32]. In the present work, we introduce Au-modified TiO_2 photocatalyst prepared and examined by the same methods as were the Ag-modified samples. We used unmodified TiO_2 P25 (Degussa) as reference catalyst and supported TiO_2, Ag- and Au-modified TiO_2 catalysts by zirconium oxide and layered silicate (sodium hectorite) mixture in the ratio of 9:1. These materials are almost completely transparent in near-UV and in visible light, thus catalysts can be excited by the incoming light without much loss of the photon energy. Zirconium oxide has also been used as a photocatalyst due to its nature as an n-type semiconductor [33,34]. Sodium hectorite has a very high specific surface area (ca. 300 $m^2\,g^{-1}$) for adsorption of pollutants, which is advantageous in heterogeneous photocatalytic system. Photocatalytic activity of pure catalyst films and hybrid composite films were studied by measuring the degradation of ethanol vapour under visible light rich light source ($\lambda \geq 435$ nm).

2. Material and methods

2.1. Sample preparation

TiO_2 (Degussa P25) with a specific BET surface area of 50 $m^2\,g^{-1}$ was used as a standard photocatalyst without any treatment. Ag- and Au-nanoparticles were placed on the surface of TiO_2 by photodeposition. 1 g of TiO_2 was dispersed either in 500 mL of 9.38×10^{-5} mol L^{-1} $AgNO_3$ (Molar, Hungary) or 500 mL of 5.1×10^{-5} mol L^{-1} $HAuCl_4{\cdot}3H_2O$ (Sigma–Aldrich) solution for Ag-TiO_2 and Au-TiO_2, respectively. Next 200 mL of 2-propanol (Molar, Hungary) was added as a sacrificial donor to promote the photoreduction of Ag^+ and Au^{3+} ions under UV light illumination by a 300 W Xe-lamp (Hamamtsu L8251, Japan) under 1 h while continuous stirring. Hybrid films were prepared by suspending the powder mixture of the catalysts and the supporting materials, which were zirconium oxide (Riedel-de Haën, purum) and sodium hectorite (Fa-Laponite, Solvay). Hybrid films containing 20%; 40%; 60%; 80%; 100% of photocatalyst with a constant mass ratio of the supporting materials (ZrO_2:hectorite = 9:1) were then prepared by spray coating technique. The thickness of the layers was measured by Elcometer 224 type digital profile gauge and found to be 10 ± 2 μm.

200 mL of silver sol was prepared with the concentration of 4.63×10^{-3} mol L^{-1} by the followings: 0.2 g of PVP (polyvinylpyrrolidone) K30 polymer was solved in 152 mL of water (0.13 wt%/V). 0.1575 g of $AgNO_3$ was solved in 8 mL of water ($c = 1.16$ mol L^{-1}) and then it was poured into the polymer solution. Finally, we added 40 mL of $NaBH_4$ solution with the concentration of 2.31×10^{-2} mol L^{-1} to the system, under intensive stirring, drop by drop.

2.2. Sample characterisation

For optical characterisation NanoCalc 2000 Micropack spectrometer equipped with an integrated sphere and HPX 2000 Mikropack high power xenon lamp were used to record the diffuse reflectance spectra (DRS) of the modified and pure TiO_2 films. Ocean Optics USB2000 diode array spectrophotometer was used to detect absorbance.

X-ray diffraction experiments were made on a Bruker DC 8 Advances diffractometer, using Cu Kα-radiation ($\lambda = 0.1542$ nm).

The specific surface area of the catalysts and the supporting materials were determined by the BET method from N_2 adsorption isotherms at 77.0 ± 0.5 K (Micrometrics Gemini 2375 Surface Area Analyser). Before the adsorption run the samples were evacuated (1.33 mPa) at 100 °C overnight.

Photooxidation of ethanol vapour on catalyst films was performed in a circulation reactor (volume c.a. 165 mL) at 25.0 ± 0.1 °C. The light source of the reactor was a 15 W low pressure mercury lamp (Light-Tech, Hungary) with an intensity of 1.26×10^{-6} einstein/s. It has characteristic emission wavelengths mostly above 435 nm. It also has emission lines at 353 and 393 nm, but only with a very low intensity. The photoreactor was covered with a quartz plate, so all the emission lines of the light source were used for the experiments. However we also examined the photocatalytic activity when wavelengths of higher energies in the near-UV were filtered using a glass plate. The light source was fixed at 50 mm distance from the films. After injection of ethanol and water vapour, the system was left to stand 30 min for the establishment of adsorption equilibrium on the surface of films. The composition of vapour phase was analysed by gas chromatograph (Shimadzu GC-14B) equipped with a thermal conductivity (TCD) and a flame ionisation detector (FID). The flow rate of the gas mixture in the photoreactor system was 375 mL min^{-1}. The initial concentration of ethanol was 0.36 ± 0.018 mmol L^{-1} at relative humidity of ~70%.

GC–MS experiments were carried out for analysing the side products on pure TiO_2 and on Au-TiO_2 films under visible light. The gas chromatograph was Shimadzu GC 2010 equipment connected to Shimadzu 2010 QP 2010 S type mass spectrometer. For separating the generated compounds HP-PLOT-Q capillary column and He carrier gas were used.

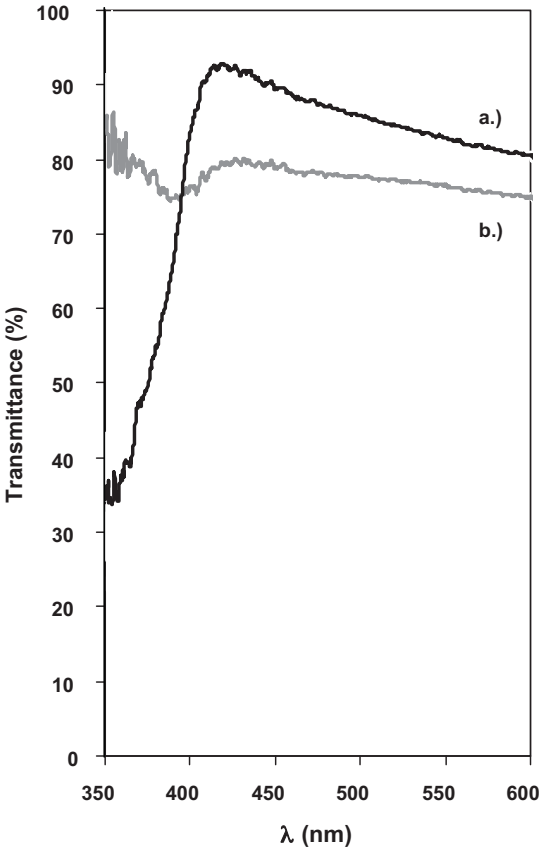

Fig. 1. Transmittance spectra of TiO_2 (a) and supports in a composition of ZrO_2:hectorite = 9:1 (b).

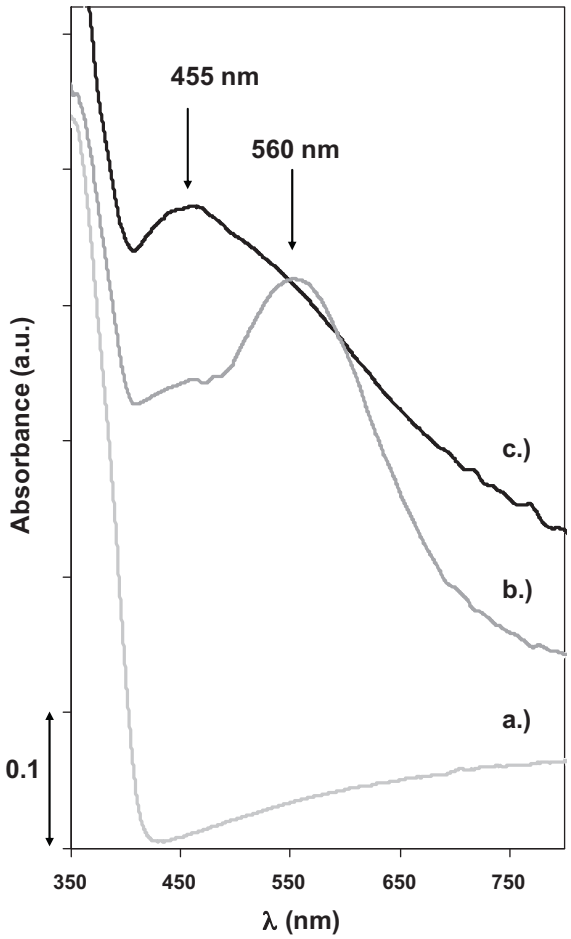

Fig. 2. Absorbance spectra of TiO_2 (a), Au-TiO_2 (b) and Ag-TiO_2 catalysts (c).

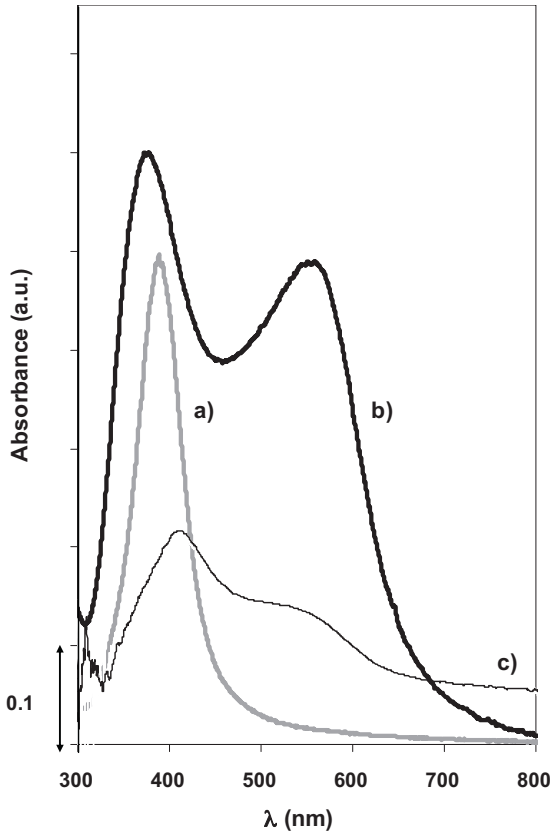

Fig. 3. Absorbance spectra of primary Ag NPs in stable aqueous dispersion (a), aggregated Ag NPs in aqueous dispersion (b) and Ag NPs on nanofilm, prepared by spray coating, on glass surface (c).

3. Results and discussion

3.1. Surface and optical properties of catalysts and hybrid films

The specific surface areas of the catalysts and supports were detected by N_2 sorption measurements and offered to be 50 $m^2\,g^{-1}$ for Degussa P25, 49.3 $m^2\,g^{-1}$ for Ag-TiO_2 and 47.8 $m^2\,g^{-1}$ for Au-TiO_2. Due to the Ag- and Au-modification the specific surface area of P25 TiO_2 decreased 0.7% and 2.2%, respectively. ZrO_2 has a relatively small specific surface area of 5.6 $m^2\,g^{-1}$; however sodium hectorite has a very high specific surface area of 305.0 $m^2\,g^{-1}$ due to its lamellar structure.

Optical properties of the supports, pure and modified catalysts are determined by the diffuse reflectance spectra, which are demonstrated in Figs. 1 and 2 The calculated transmission of the supports are 80–90% in the UV–vis range of the spectrum, thus photons of these ranges can be utilised to excite TiO_2. The prepared layer in the composition of ZrO_2:hectorite = 9:1 transmits 80% of the incoming light (Fig. 1). Due to the modification of TiO_2 with Ag and Au NPs, the colour of samples changed from white to brownish or purple. This change resulted a broadened peak in case of the Ag-modified sample, which appeared in the visible range from about 400 to 650 nm with a maximum at 455 nm. The Au-modified sample also possessed a peak from 490 to 750 nm with a maximum of 560 nm (Fig. 2). This phenomenon is affected by the plasmonic properties of Ag and Au NPs at localised surface plasmon resonance wavelengths. It is well-known that the position and absorbance maximum of the surface plasmon band of noble metal NPs depends on the shape, size, composition and aggregation state of the particles' assemblies [35–38]. Besides the characteristic surface plasmon band of NPs, a new band, which appears at higher wavelength, always corresponds to the formation of larger and/or ellipsoidal and/or aggregated particles [39] in the system, but this observation also may indicate reduced interparticle distance [40]. To explain the surface structure of adhered noble metal NPs, we have investigated their plasmonic properties in aqueous dispersion and in thin film on solid glass surface, prepared by spray coating. In the case of primary Ag NPs in aqueous dispersion the representative plasmon band appears between ~380 and 420 nm in the UV–vis spectrum depending on the size of particles. Fig. 3 shows a typical absorbance band of PVP-stabilized Ag nanodispersion at λ_{max} = 390 nm (Fig. 3 curve a). When the dispersion aggregates, a shoulder appears at about 550–560 nm. A representative absorption spectrum of an aggregated silver sol can be seen in Fig. 3 curve b. Also aggregation occurs, when preparing a nanofilm from a sol containing primary Ag NPs. Due to the film preparation of PVP-stabilized Ag NPs on glass support, the plasmon band of primary spherical NPs (Fig. 3 curve c) shifted from λ_{max} = 390 nm to λ_{max} = 415 nm. Moreover, a new absorbance shoulder appeared near λ = 550 nm. It corresponds to the formation of Ag NP aggregates, similarly to the aggregated Ag dispersion (Fig. 3 curves b and c).

Based on the results of previously published articles [36,37] the plasmon maximum at λ_{max} = 455 nm corresponds to the characteristic plasmon band of Ag-modified TiO_2 (Fig. 2 curve c.). As it can be seen a shoulder is also observed at around λ = 550 nm. As it was previously mentioned in the case of PVP-stabilized silver nanofilm, most probably one part of the Ag NPs migrated on the surface of TiO_2 during the preparation, and this aggregation effect can be seen in the nanofilm as well. Detailed data of XRD and XPS measurements of silver modified sample are presented in our pre-

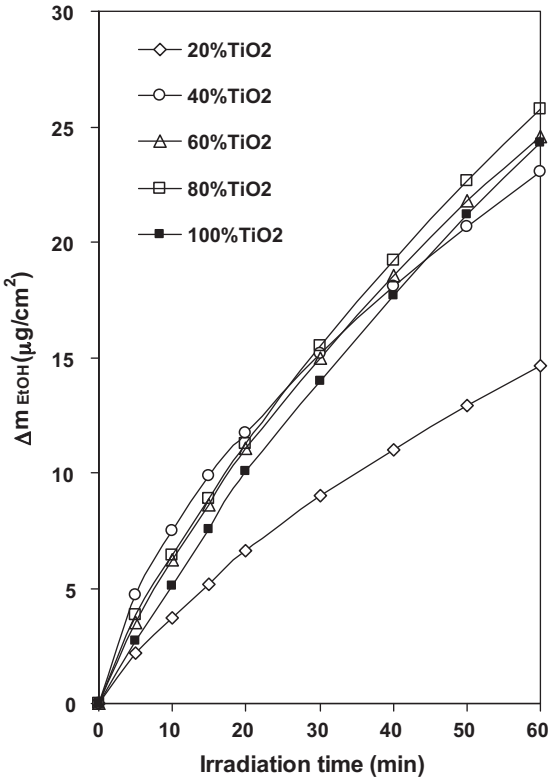

Fig. 4. Photooxidation of ethanol under visible light ($\lambda \geq 435$ nm) on P25 TiO_2 hybrid films containing ZrO_2:hectorite = 9:1 supports.

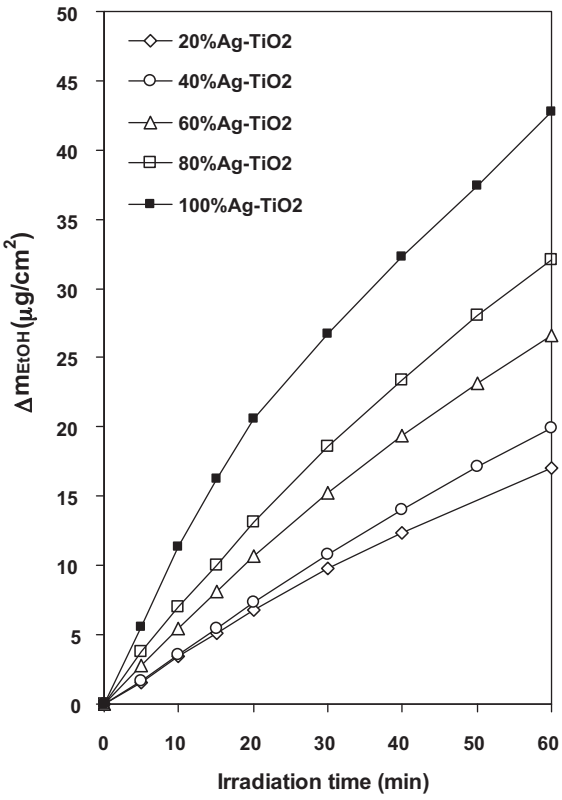

Fig. 5. Photooxidation of ethanol under visible light ($\lambda \geq 435$ nm) on Ag-TiO_2 hybrid films containing ZrO_2:hectorite = 9:1 supports.

vious publication [32]. XRD measurements revealed 87% of anatase and 13% of rutile phase of TiO_2, but not any characteristic reflection of crystalline silver, silver oxide or metal gold in the modified samples. Based on XRD results, XPS revealed silver oxide phase. Azizi et al. and Do et al. investigated the high resolution XP spectra of regions of Ti 2p O 1s and Au 4f of the gold modified samples. There is a doublet in the spectrum of Au $4f_{7/2}$ energy level around 83.8 eV indicating the presence of metal gold on TiO_2 surface [41,42].

3.2. Photocatalytic efficiency

The photocatalytic efficiency of hybrid films was measured for ethanol oxidation at a relative humidity of ~70% and at $25.0 \pm 0.1\,^{\circ}C$. The reference catalyst films were pure P25 TiO_2, Ag- and Au-modified TiO_2 catalyst without any supporting material. We repeated the photocatalytic experiments and the results were reproducible within ±5%. There was no ethanol degradation at the absence of catalyst hybrid film; therefore self-photolysis could be excluded. Using a glass window on the reactor ($\lambda > 350$ nm) resulted 17.4% worse conversion of ethanol on 80% Ag-TiO_2 hybrid catalyst film catalyst, due to cutting off the emission wavelengths of the lamp in the near-UV range. Curves presenting the decomposition of ethanol on pure catalysts and on hybrid films are presented in Figs. 4–6. Pure Ag-TiO_2 catalyst film was found to be the most effective with a degradation of 42.73 $\mu g/cm^2$ ethanol. Pure TiO_2 P25 and Au-TiO_2 degraded 24.33 and 32.31 $\mu g/cm^2$ ethanol, respectively. Hybrid films prepared with modified catalysts performed higher efficiencies than TiO_2 hybrid films (Fig. 7).

The degradations followed pseudo-first order kinetics, evaluated from $\ln(c_0/c)$ vs. irradiation time representation. The apparent reaction rate constants and the correlation coefficients of the linear pseudo-first order interpolations are shown in Table 1. In case of Ag-TiO_2 catalyst, photocatalytic efficiency nearly linearly increased with increasing amount of catalyst in the hybrid films.

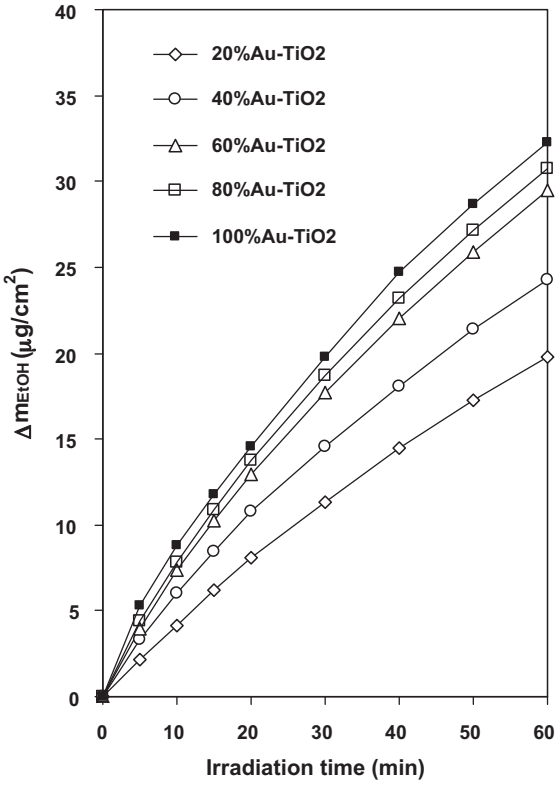

Fig. 6. Photooxidation of ethanol under visible light ($\lambda \geq 435$ nm) on Au-TiO_2 hybrid films containing ZrO_2:hectorite = 9:1 supports.

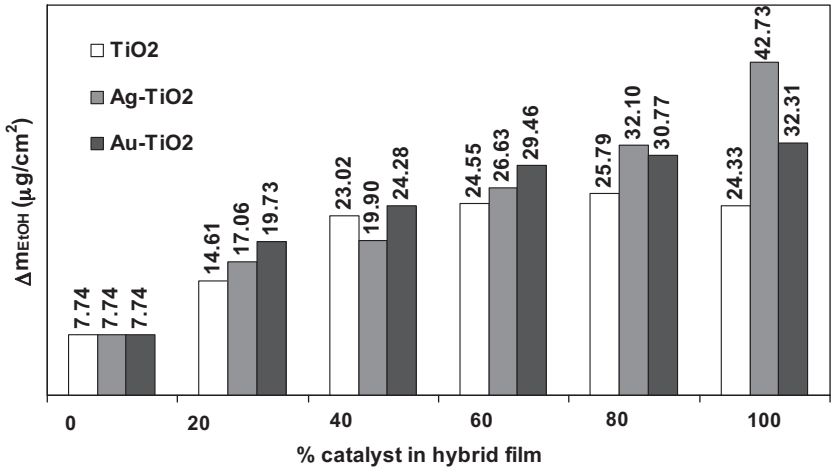

Fig. 7. Photooxidation of ethanol on TiO_2, Ag-TiO_2 and Au-TiO_2 hybrid films.

As for Au-TiO_2 hybrid films, the photocatalytic efficiency stopped to improve significantly above 60% of catalyst content. In contrary, TiO_2 reached maximal photocatalytic degradation rate already at 60% of catalyst content, as shown in Figs. 7 and 8.

Since adsorption of the supports takes important part in the photocatalysis, we followed the adsorbed amounts of ethanol on the films (see Fig. 8). The most significant ethanol adsorption was found on films containing 60% and 80% of supports. The adsorption of ethanol vapour on thin nanohybrid films was calculated by the following formula (Eq. (1)):

$$n^s = \frac{(c_0 - c_{0'})V_{\text{reactor}}}{A^s_{\text{film}}} \quad (1)$$

where c_0 is the initial concentration of ethanol; $c_{0'}$ is the concentration of ethanol after 30 min of circulation in the system in dark, to reach the adsorption equilibrium; V_{reactor} is the total volume of the adsorption space and A^s_{film} is the reactive surface area of the nanocomposite film. On the hybrid films with high support content (at 20–40 wt% of catalyst content) there is a maximum adsorption of ethanol, which aids the photocatalytic processes. The amount of decomposed ethanol on hybrid film was compared to the amount of decomposed ethanol on pure TiO_2 without any supporting materials. Since, composite films contained 20; 40; 60; 80 wt% of catalysts, the reference value was corrected in accordance with the catalyst content (w_1) in the different hybrid films. In this way, a synergistic effect could be calculated by Eq. (2).

$$\text{Synergistic effect} = \frac{\Delta c_{(\text{EtOH})\text{hybrid film (measured)}} - \Delta c_{(\text{EtOH) support (measured)}}}{w_1 \Delta c_{(\text{EtOH})\text{TiO}_2}} \times 100. \quad (2)$$

The synergistic effect is a result of the advantageous properties of supports and, in case of Ag- and Au-TiO_2 films, there is an additional favourable effect of the plasmonic catalysts on the photocatalytic rate. The $\Delta c_{(\text{EtOH) hybrid film (measured)}}$ is the decrease in ethanol concentration produced by the hybrid film in 60 min, the $\Delta c_{(\text{EtOH) support (measured)}}$ is the decrease in ethanol concentration produced by the supports without any catalyst in 60 min. The $w_1 \Delta c_{(\text{EtOH})\text{TiO}_2}$ is a theoretical value, which denotes the degradation of ethanol on pure TiO_2 P25 film after 60 min, based on the mass ratio of the catalyst content in the hybrid film. There is a specific enhancement on 20–80% of TiO_2 hybrid films due to the supports, as shown in Fig. 9. An additional favourable effect can be found on Ag- and Au-TiO_2 hybrid films, which is the joint effect of supports and plasmonic catalysts (see Fig. 9).

We also carried out GC–MS experiments on pure P25 TiO_2 and on Au-TiO_2 photocatalyst films to monitor the degradation of ethanol and the generated intermediates. Qualitative results of GC–MS can be found in Table 2. Some products appear as intermediates, and then decompose into other products. The first intermediate appeared was acetaldehyde. The maximal concentration of acetaldehyde was measured in the 60th minute of irradiation. This concentration of acetaldehyde was equal to 27.0% of the initial molar amount of ethanol. No carbon dioxide was detected after 1 h of irradiation. On gold modified TiO_2, however, maximal concentration of acetaldehyde was detected after 55 min of irradiation and this amount was equal to 31.0% of the initial molar amount of ethanol. Carbon dioxide appeared after 10 min of illumination on Au-TiO_2, but only 2.6% of ethanol was mineralised into carbon

Table 1
Kinetic constants and the correlation coefficients of the linear pseudo-first order interpolations.

% Catalyst in hybrid film	k (1/min)	R^2
0% catalyst	0.0028	0.9912
20% TiO_2	0.0091	0.9910
40% TiO_2	0.0129	0.9696
60% TiO_2	0.0113	0.9958
80% TiO_2	0.0122	0.9979
100% TiO_2	0.0107	0.9999
20% Ag-TiO_2	0.0085	0.9996
40% Ag-TiO_2	0.0104	0.9959
60% Ag-TiO_2	0.0133	0.9981
80% Ag-TiO_2	0.0149	0.9976
100% Ag-TiO_2	0.0266	0.9850
20% Au-TiO_2	0.0092	0.9998
40% Au-TiO_2	0.0121	0.9980
60% Au-TiO_2	0.0144	0.9992
80% Au-TiO_2	0.0156	0.9992
100% Au-TiO_2	0.0175	0.9984

Table 2
Results of GC–MS qualitative analysis of ethanol photodegradation for different intermediates.

Species	Chemical composition	Retention time (min)
Carbon monoxide	CO	1.923
Methane	CH_4	2.013
Carbon dioxide	CO_2	2.384
Ethane	C_2H_6	3.093
Acetaldehyde	CH_3CHO	5.990
Ethanol	C_2H_5OH	7.212
Acetone	CH_3COCH_3	8.018
Ethyl acetate	$C_4H_8O_2$	10.920
Methyl formate	$HCOOCH_3$	6.574
Ethyl formate	$C_3H_6O_2$	8.384

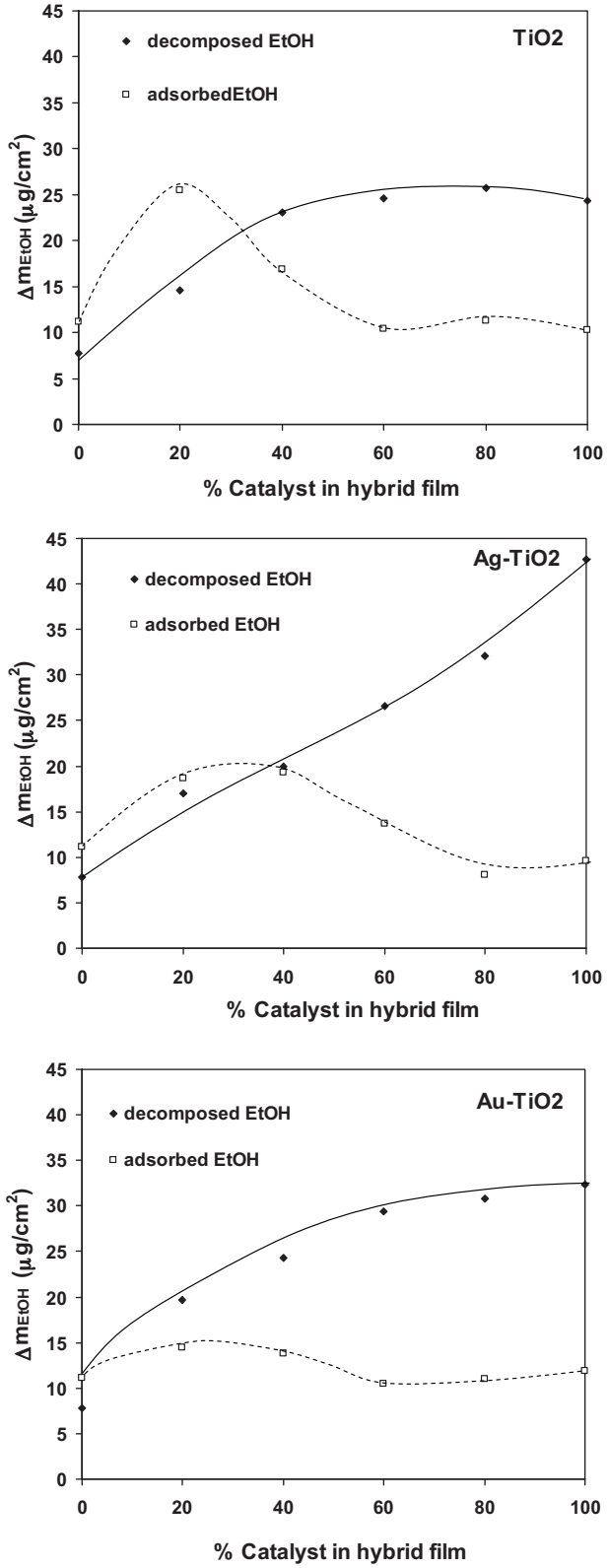

Fig. 8. The adsorbed and photodegraded amount of ethanol on TiO_2, Ag-TiO_2 and Au-TiO_2 hybrid films.

dioxide after 60 min. Ethyl formate and ethyl acetate also appeared in small amounts (~2.5%) on both catalysts. The main differences between TiO_2 and Au-TiO_2 were that carbon dioxide, acetone and ethane appeared on Au-TiO_2 after 60 min of irradiation, but not on untreated TiO_2 P25.

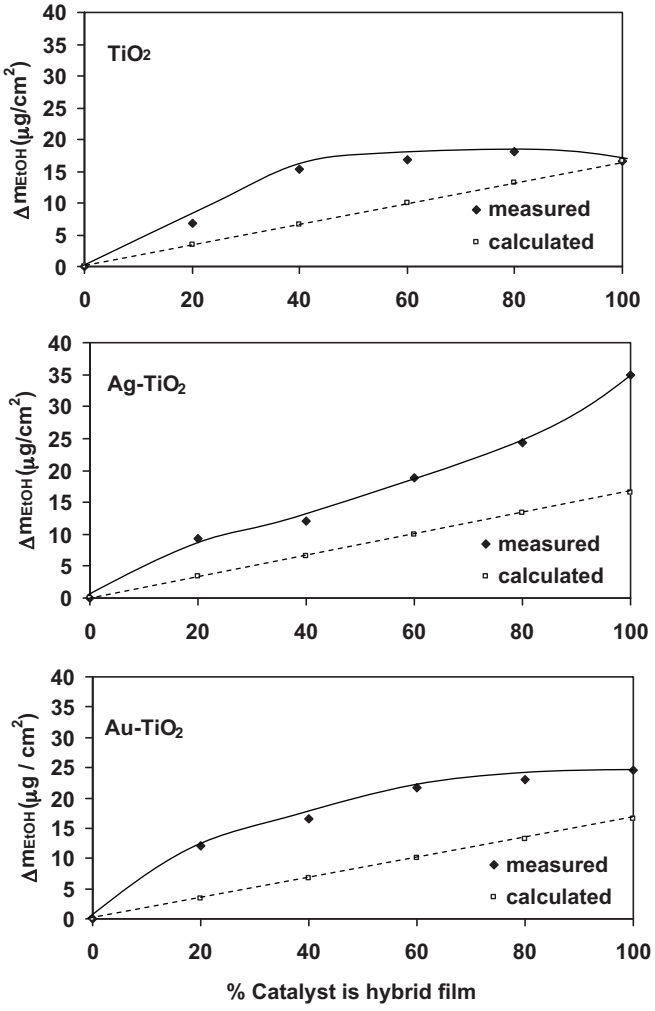

Fig. 9. Measured and the calculated Δm_{EtOH} amount as a function of hybrid film composition. The synergistic effect is calculated by Eq. (2).

4. Conclusions

The optical and photocatalytic properties of pure TiO_2, Ag- and Au-TiO_2 catalysts and of their supported films were compared in this study. The supports were optically transparent zirconium oxide and sodium hectorite layer silicate. Ag and Au NPs significantly increased the rate of ethanol degradation. It is presumably caused by the plasmonic absorbance of noble metal NPs and reduced rate of electron–hole pair combination. Supporting materials with 80–90% transmittance and a significant adsorption capacity had a favourable effect on the photocatalytic process. The Ag- and Au-modified catalysts enhanced the photocatalytic rate by their plasmonic properties. These findings together result the synergistic effect of the reactive nanohybrid films.

Acknowledgements

This work was partially financed by the Hungarian National Office of Research and Technology (NKTH) under contract no. TECH-09-A2-2009-0129 (NANOSTER) and the European Regional Fund who co-financed the project named "TÁMOP-4.2.1/B-09/1/KONV-2010-0005 – Creating the Center of Excellence at the University of Szeged" with the European Union.

References

[1] G. Rothenberger, J. Moser, M. Grätzel, N. Serpone, D.K. Sharama, J. Am. Chem. Soc. 107 (1985) 8054–8059.
[2] Y.R. Do, W. Lee, K. Dwight, A. Wold, J. Solid State Chem. 108 (1994) 198–201.
[3] S. Sakthivel, H. Kisch, Angew. Chem. Int. Ed. 42 (2003) 4908–4911.
[4] R. Kun, S. Tarján, A. Oszkó, T. Seemann, V. Zöllmer, M. Busse, I. Dékány, J. Solid State Chem. 182 (2009) 3076–3084.
[5] L. Kőrösi, Sz. Papp, I. Bertóti, I. Dékány, Chem. Mater. 19 (2007) 4811–4819.
[6] L. Kőrösi, A. Oszkó, G. Galbács, A. Richardt, V. Zöllmer, I. Dékány, Appl. Catal. B 77 (2007) 175–183.
[7] L. Kőrösi, I. Dékány, Colloids Surf. A 280 (2006) 146–154.
[8] T. Yamaki, T. Sumita, S. Yamamoto, J. Mater. Sci. Lett. 21 (2002) 33–35.
[9] C. Adán, J. Carbajo, A. Bahamonde, A. Martínez-Arias, Catal. Today 143 (2009) 247–252.
[10] B. Xin, Z. Ren, P. Wang, J.L.L. Jing, H. Fu, Appl. Surf. Sci. 253 (2007) 4390–4395.
[11] H. Irie, T. Shibanuma, K. Kamiya, S. Miura, T. Yokoyama, K. Hashimoto, Appl. Catal. B 96 (2010) 142–147.
[12] S.D. Sharma, D. Singh, K.K. Saini, C. Kant, V. Sharma, S.C. Jain, C.P. Sharma, Appl. Catal. A 314 (2006) 40–46.
[13] S. Sakthivel, M.V. Shankar, M. Palanichamy, B. Arabindoo, D.W. Bahnemann, V. Murugesan, Water Res. 38 (2004) 3001–3008.
[14] A. Kafizas, S. Kellici, J.A. Darr, I.P. Parkin, J. Photochem. Photobiol. A 204 (2009) 183–190.
[15] A. Zielińska, E. Kowalska, J.W. Sobczak, I. Łącka, M. Gazda, B. Ohtani, J. Hupka, A. Zaleska, Sep. Purif. Technol. 72 (2010) 309–318.
[16] R.S. Sonawane, M.K. Dongare, J. Mol. Catal. A 243 (2006) 68–76.
[17] P.S.S. Kumar, R. Sivakumar, S. Anandan, J. Madhavan, P. Maruthamuthu, M. Ashokkumar, Water Res. 42 (2008) 4878–4884.
[18] V. Subramanian, E. Wolf, P.V. Kamat, J. Phys. Chem. B 150 (2001) 11439–11446.
[19] W. Hou, Z. Liu, P. Pavaskar, W.H. Huang, S.B. Cronin, J. Catal. 277 (2011) 149–153.
[20] H.M. Sung-Suh, J.R. Choi, H.J. Hah, S.M. Koo, Y.C. Bae, J. Photochem. Photobiol. A 163 (2004) 37–44.
[21] J.C. Colmenares, M.A. Aramendía, A. Marinas, J.M. Marinas, F.J. Urbano, Appl. Catal. A 306 (2006) 120–127.
[22] B. Kraeutler, A.J. Bard, J. Am. Chem. Soc. 100 (1978) 5985–5992.
[23] J. Lee, W. Choi, J. Phys. Chem. B 109 (2005) 7399–7406.
[24] J. Sá, M. Fernandez-Garzia, J.A. Anderson, Catal. Commun. 9 (2008) 1991–1995.
[25] K. Awazu, M. Fujimaki, C. Rockstuhl, J. Tominaga, H. Murakami, Y. Ohki, N. Yoshida, T. Watanabe, J. Am. Chem. Soc. 130 (2008) 1676–1680.
[26] M. Mrowetz, A. Villa, L. Prati, E. Selli, Gold Bull. 40 (2007) 154–160.
[27] B.K. Min, J.E. Heo, N.K. Youn, O.S. Joo, H. Lee, J.H. Kim, H.S. Kim, Catal. Commun. 10 (2009) 712–715.
[28] R. Chatti, S. Rayalu, N. Dubey, N. Labhsetwar, S. Devotta, Sol. Energy Mater. Sol. Cells 91 (2007) 180–190.
[29] E. Carpio, P. Zúñiga, S. Ponce, J. Solis, J. Rodriguez, W. Estrada, J. Mol. Catal. A 228 (2005) 293–298.
[30] R. Kun, M. Szekeres, I. Dékány, Appl. Catal. B 68 (2006) 49–58.
[31] J. Ménesi, L. Kőrösi, É. Bazsó, V. Zöllmer, A. Richardt, I. Dékány, Chemosphere 70 (2008) 538–542.
[32] L. Kőrösi, Sz. Papp, J. Ménesi, E. Illés, V. Zöllmer, A. Richardt, I. Dékány, Colloids Surf. A 319 (2008) 136–142.
[33] C. Karunakaran, S. Senthilvelan, J. Mol. Catal. A 233 (2005) 1–8.
[34] B. Neppolian, H.C. Choi, S. Sakthivel, B. Arabindoo, V. Murugesan, J. Hazard. Mater. 89 (2002) 303–317.
[35] W. Haiss, N.T.K. Thanh, J. Aveyard, D.G. Fernig, Anal. Chem. 79 (2007) 4215–4221.
[36] L.M. Liz-Marzán, Langmuir 22 (2006) 32.
[37] Z. Zhong, S. Patskovskyy, P. Bouvrette, J.H.T. Luong, A. Gedanken, J. Phys. Chem. B 108 (2004) 4046.
[38] A. Majzik, R. Patakfalvi, V. Hornok, I. Dékány, Gold Bull. 42 (2009) 113–123.
[39] H.H. Huang, X.P. Ni, G.L. Loy, C.H. Chew, K.L. Tan, F.C. Loh, J.F. Deng, G.Q. Xu, Langmuir 12 (1996) 909–912.
[40] J.A. Schuller, E.S. Barnard, W. Cai, Y. Jun, J.S. White, M.l. Brongersma, Nat. Mater. 9 (2010) 193.
[41] Y. Azizi, V. Pitchon, Appl. Catal. A 385 (2010) 170–177.
[42] Y. Do, J.-S. Choi, S.K. Kim, Y. Sohn, Bull. Korean Chem. Soc. 31 (2011) 2170–2174.